# First 3D modeling of tungsten erosion and migration in WEST discharges adopting a toroidally non-symmetric wall geometry

S. Di Genova [1], G. Ciraolo[2], A. Gallo[2], J. Romazanov[3], N. Fedorczak[2], H. Bufferand[2], P. Tamain[2], N. Rivals[2], Y. Marandet[4], S. Brezinsek[3], E. Serre[1] and the WEST team[5]

[1]M2P2, Aix-Marseille Univ, CNRS, Centrale Marseille, 13013 Marseille,France
[2]IRFM, CEA-Cadarache, 13108 Saint-Paul-lez-Durance, France
[3]IEK-4, Forschungszentrum Jülich, 52425 Jülich , Germany
[4]PIIM, Aix-Marseille Univ, CNRS, 13013 Marseille, France
[5]http://irfm.cea.fr/en/west/WESTteam/

**Abstract**

Numerical analysis is a useful tool to investigate tungsten (W) sources and transport across plasma in W Environment Steady-State Tokamak (WEST) plasma discharges, as it can highlight physical mechanisms not always directly measurable in experiments. Modelling activity was performed to study W erosion from WEST plasma-facing components (PFCs), as well as W migration through plasma. For the first time it was adopted a toroidally asymmetric wall geometry formed by toroidally localized objects representing WEST outer limiter or antennas. 3D non-axisymmetric SOLEDGE transport simulations were performed with simplifying assumptions (pure Deuterium plasma, fluid model for neutrals) to simulate WEST boundary plasma, and then used as background for ERO2.0 runs to model W erosion, re-deposition, and migration. On the sides of the toroidally localized objects, two thin W stripes were considered in order to model WEST W antennas protections. Simulations suggest that particles eroded from the antennas protections may dominate core W contamination in the analysed wall configuration. Hence, results encourage to adopt

3D non-axisymmetric models on a wider set of plasma conditions and wall configurations to further investigate the relevance of toroidally localized objects to WEST W ions plasma contamination.

# 1 Introduction

The capability of studying heavy elements erosion and migration in tokamaks represents an important help to current and next generation fusion experiments. Tungsten (W) is considered to be the most suitable material to cover walls and interface plasma in future reactors. It has been widely tested in tokamaks such as ASDEX [1] and JET-ILW [2]. Some of the Tungsten Environment Steady-state Tokamak (WEST) [3] main goals are to study the feasibility of using W in steady operations, being a long pulse machine, and to test the divertor monoblocks that will be adopted for ITER. WEST operations are largely influenced by W erosion and migration into the confined plasma, as W represent the bulk material for the divertor monoblocks and the coating material for all the Plasma Facing Components (PFCs). Some PFCs are toroidally localized objects, as shown in figure 1a. Among those toroidally localized PFCs, some components surface is usually located close to the hot confined plasma, acting as limiters. WEST limiters in discharges start-up, or the radio frequency (RF) antennas protections during discharges, are strongly eroded [4] and suspected to have a predominant impact in influencing WEST core W content.
In previous contributions, numerical modelling activity was performed in order to study W erosion and migration at WEST PFCs [5–7] under the assumption of axisymmetric wall geometry. In this work we introduce for the first time numerical analyses of W erosion and migration in WEST using 3D simulations of an asymmetric wall geometry composed of both axisymmetric PFCs and toroidally localized objects, as shown in figure 1b. We here describe a set-up for SOLEDGE [8] and ERO2.0 [9] simulations representing WEST discharges in which the impact of toroidally localized object is supposed to be particularly important to W core contamination, due to a specific choice of the radial gap between the separatrix and the antennas. The discussion of the results follows.

# 2 Model wall geometry

The model wall geometry was updated from a previous axisymmetric one, the former axisymmetric wall had a single wide toroidal outer limiter (i.e. an

axisymmetric toroidal ring) as shown in figure 2. As the axisymmetric limiter surface was way greater than the surface of interaction of WEST limiters or antennas with plasma, the outboard limiter was retracted of distance of roughly 20 cm to avoid overestimating plasma recycling and W erosion as described in [6]. This distance was not chosen with any particular criteria and it is worth it to highlight that it is way larger than the usual WEST gaps between the confined plasma and the closer PFCs, e.g. the antennas have a distance from the separatrix between 1 cm and 5 cm when RF power is injected [4]. Due to its gap from the main separatrix, the limiter contribution to the overall core W content in simulations was often negligible [5], underlining the intricacy in studying the effects of WEST outboard limiter and antennas using 2D axysimmetric simulations. Performing an update to a new non-axysimmetric wall geometry with toroidally localized objects (see figure 3) was possible thanks to new SOLEDGE developments allowing 3D asymmetric simulations [10]. The new wall was provided by four toroidally localized antennas. Each of the four antennas was located 90° from the next ones, with their distance from the separatrix of the considered magnetic configuration being about 1.5 cm. In WEST experiments the gap between separatrix and the first object in the Low Field Side (LFS) is on average roughly 3 cm, but values between 1cm and 2 cm are not excluded [4], so the distance considered here can be seen as a lower limit.
The wall PFCs were divided in three different types as shown in figure 3: The Axisymmetric ones (grey objects in the figure) were always considered W sources. The ones consisting of the body of the antennas (black objects in the figure, 10° wide each) were never considered W sources, as they were aimed to represent the antennas central components made of middle Z elements, as silver (Ag) and copper (Cu). Finally, the ones consisting of the sides of antennas (red objects in the figure, 3.5° wide each) were not considered W sources in a first simulation and then used as W source in a second run to study their impact on the overall W core content. The purpose of those PFCs was to model W antennas protections present in WEST. For what concerns W deposition, there was no difference between any of the PFCs in the simulations.
Due to technological limitations that will be discussed in the next section, in this model the wall surfaces were either parallel or orthogonal to the toroidal direction, so they were intersected by the toroidal component of the magnetic field with an azimuthal angle that could be either 0°, as the axisymmetric components, or 90°, as the side surfaces of the antennas (however, the presence of the poloidal component of the magnetic field prevented having null intersection between the field and the wall). For this reason, the actual curved "bumping" shape of the antennas protections could not be here reproduced,

and the magnetic field intersects the sides of the antennas protections nearly orthogonally.

# 3 Boundary plasma modelling

Boundary plasma was modelled through SOLEDGE [8, 10]. SOLEDGE is capable of solving fluid mass, momentun, and energy balance equations for multiple species from the edge plasma up to the first wall in complex geometries. SOLEDGE adopts flux-surface aligned structured mesh in which quadrangles in the poloidal plane are extruded in the toroidal direction. The wall geometry is imposed through boundary conditions immersed inside the mesh, so the wall surfaces can't be tilted with respect to the toroidal direction as explained in the previous section.
The simulation here described was in pure deuterium (D), turbulent phenomena were accounted only on "large" tokamak scales through diffusive processes (i.e. a transport simulation) adopting mean-field transport coefficients for particle cross-field diffusion $D_\perp$ and viscosity $\nu_\perp$ such as : $D_\perp = \nu_\perp = 0.3$ m$^2$/s, and cross-field heat conductivity for ions $\chi^{\mathrm{i}}_\perp$ and electrons $\chi^{\mathrm{e}}_\perp$ such as: $\chi^{\mathrm{i}}_\perp = \chi^{\mathrm{e}}_\perp = 1$ m$^2$/s. Drifts were not included in the runs. Neutrals physics was handled with a single diffusive fluid model in SOLEDGDE itself, as the coupling between SOLEDGE and EIRENE, accomplished in 2D simulations [8], is still in development for 3D simulations at the moment of writing of this document.
The total power entering in the scrape-off layer $P_{\mathrm{SOL}}$ was set to 1MW, the electron density $n_{\mathrm{e}}$ at the core-edge interface (the simulation inner boundary) was set to $5 \times 10^{19}$ m$^{-3}$, and a neutral gas injection rate (or puff) of $7 \times 10^{20}$ s$^{-1}$ was located in the private flux region, the recycling coefficient was set to be on whole wall surface equal to 97% (lower than the usual values used for W surfaces to taking into account the pumps effect on neutrals).
The simulation domain was symmetric with respect to a quarter of torus, the quarter of torus toroidal discretization consisted of 32 sectors of roughly 0.05 rad each (2.81°).
Representative figures of the 3D simulation can be found in figures 4 and 5. Figure 5 represents the parallel velocity field in a poloidal cross section of the torus. At LFS Plasma flow goes axysimmetrially in the magnetic field direction at the top of the machine, and in the opposite direction at the bottom. The presence of toroidally localized objects breaks the axisymmetry with plasma flowing in opposite directions at the two sides of the antenna. This effect can't be reproduced in 2D simulations. Despite the simplified model, SOLEDGE results were realistically inside WEST operational space

in L-mode [5,11,12], with values that could be the ones of a typical WEST discharge: figure 6 and 7 show density and temperature at outer midplane and divertor targets respectively in the simulation, at a toroidal angle halfway between two antennas : $n_e$ at the outer midplane separatrix was $2.5\times10^{19}$ [$m^{-3}$], going up to $3.4 \times 10^{19}$ [$m^{-3}$] at the outer target due to recycling at divertor plates. $T_e$ went from 50 [eV] at the separatrix down to 30 [eV] at the outer target, as the plasma was in conduction limited regime. $T_i$ at antennas major radius was roughly 50 [eV] and its variation along the toroidal angle was negligible, likewise, $T_e$ modulation in the toroidal direction was also insignificant. On the other hand, plasma speed strongly varied along the toroidal field, as plasma went repeatedly from stagnant to sound speed along the magnetic lines as a results of Bohm condition at the antennas surfaces. In figure 8 plasma parallel velocity field at a major radius greater than the antennas one is shown, the field at the two sides of each antenna is not symmetrical, as the poloidal magnetic topology in the upper and the lower part of the machine is not identical. Density slightly modulates in the toroidal direction as a result of plasma recycling at antennas surface and the fact that flux along the magnetic lines is roughly conserved. In figure 9 the relative midplane toroidal modulation at antenna major radius is shown for $n_e$, $T_e$, $T_i$, and $v_\parallel$. The relative midplane toroidal modulation of a quantity $A$ at a certain value $\varphi$ of the toroidal angle is defined as $\bar{A}(\varphi) = (A(\varphi) - < A >_{2\pi})/\mathrm{Max}(A)_{2\pi}$, with the toroidal average $< ... >_{2\pi}$ and the maximum on the toroidal angle $\mathrm{Max}(...)_{2\pi}$ reported for each physical quantity in table 1.

# 4 W erosion and migration modelling

W erosion and migration was modelled through ERO2.0 [9]. ERO2.0 is a code for Monte Carlo impurity tracking and surface erosion and deposition computation. SOLEDGE results described in section 3 were used as plasma background for ERO2.0 runs. SOLEDGE and ERO2.0 simulations wall geometries were identical. Actually, ERO2.0 is capable to handle any wall geometry regardless the one used for the plasma background, so a more realistic geometry of the antennas protections could had been used, projecting SOLEDGE results on the alternative wall through some kind of interpolation. However, in this work it was preferred to keep consistency between SOLEDGE and ERO2.0 simulations wall geometries.
It is well known that W sputtered by D is negligible compared to sputtering by light impurities in L-mode discharges [13]. Uniform concentration values of oxygen (O) of 3% was set in ERO2.0 simulations as a proxy of the different light impurities usually found in WEST such as nitrogen (N), boron

(B), and carbon (C) [14]. O ionisation states abundance (i.e. relative concentration) from 1+ to 8+ was set to be equal to the values found at the WEST divertor of 2D SOLEDGE simulations in which O distribution was self-consistently computed and compared to experimental data [11]. Thompson distribution [15] was used for the energy of the sputtered particles, while a butterfly-like distribution [15] was used for the azimuthal angle of sputtered W. Turbulent transport was modelled with random cross-field displacements equal to $\sqrt{4D_{\perp}\Delta t}$ , where $\Delta t$ is the particles time-step, and $D_{\perp}$ is the diffusion coefficient, considered equal to the value used in SOLEDGE. Inside the sheath, the electrostatic potential $\phi$ followed the Borodkina model [16], a simplified version of the Chodura model [17] that allows to compute $\phi$ distribution without solving integral equations. $n_{\mathrm{e}}$ dropped proportionally to the Boltzmann factor $\exp(\mathrm{e}\phi/T_{\mathrm{e}})$ [18], where e is the electron charge. model collisional forces included kinetic formulae for both friction forces $F_0$ and thermal forces $F_{\nabla T}$ as widely described in literature [19, 20]. Contamination from W self-sputtering was not included to keep the analyses simple and linear. Outside the sheath, the electric force was neglected as it is typically smaller than collisonal forces for impurities, as it is proportional to the particles charge, whereas collisonal forces are proportional to the square of the charge [18]. $\vec{B} \times \nabla B$ drifts were self-consistently computed from Lorentz force, as well as $\vec{E} \times \vec{B}$ inside the sheath.

As explained in section 2, simulations were repeated with and without considering antennas protections W source. Figure 10 shows W density maps from the two cases results: in the case without antennas protections source, the main contribution to W content inside the confined plasma was given by the top of the machine, while in the opposite case W coming from the antennas protections dominates the core. The global picture of the density map changes between the two cases, with the edge W level being roughly one order of magnitude higher in the case including the antennas protections source. As self-sputtering was not included in simulations, the global effect of all the PFCs on the overall W core content was the superposition of the effects of the single PFCs, and the difference of density between simulations is purely caused by plasma erosion of the antennas protections. Table 2 reports the values of the total number of W particles found inside the separatrix coming from the antennas protections and from the rest of the PFCs. likewise, the erosion rate of the two groups of PFCs is also written in the table. In percentage, 85% of the erosion rate in caused by the plasma interaction with the axisymmetric PFCs (lower divertor, upper divertor, baffle, tokamak ceiling), but 90% of W particles found in the separatrix comes from the antennas protections. This result may overestimate the actual impact of

the antennas protections in experiments, as the distance from the separatrix is a lower limit. Nevertheless, the impact of the toroidal localized objects seems to be significant.

# 5 Conclusions

WEST boundary plasma, wall erosion, and W migration was modelled in a toroidally asymmetric wall geometry including toroidaly localized objects. Pure D SOLEDGE 3D simulations were carried out to reproduce plasma main species (D and e) conditions, using a simple fluid model for neutrals and diffusive processes as a proxy for turbulent transport. ERO2.0 simulations were run to model W erosion and migration, adopting a uniform concentration of O of 3% to model W sputtering by light impurities. Simulations were repeated with and without considering W erosion at antennas protections. The impact of the antennas protections on the overall W content inside the separatrix in the considered configuration suggests that taking into account toroidally localized objects may be necessary to accurately simulate boundary phenomena and impurity physics in WEST discharges, encouraging modelling activity adopting 3D toroidally asymmetric walls, improving the consistency with the experiment geometry and scanning toroidally localized objects distance from the separatrix, as well as analyse different plasma regimes and scenarios.

# Aknowldgment

This work has been carried out within the framework of the EUROfusion Consortium and has received funding from the Euratom research and training programme 2014-2018 and 2019-2020 under grant agreement No 633053. The views and opinions expressed herein do not necessarily reflect those of the European Commission.

# Figures

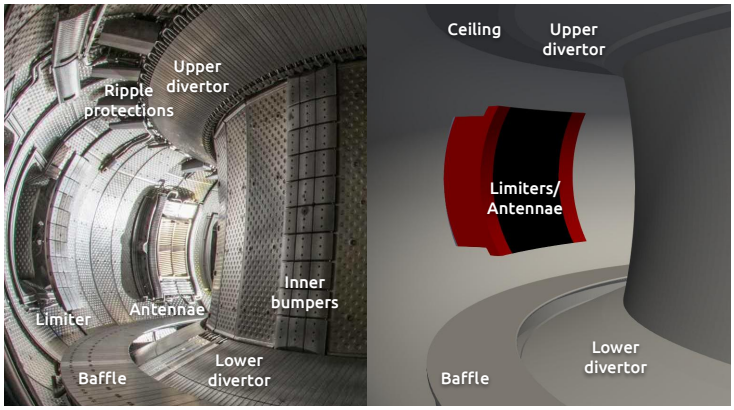


(a) (b)

Figure 1: a) WEST PFCs, completely made by bulk W, or coated with W (up to C4 campaign, 2019). Among them, some are toroidally localized objects (Inner bumpers, RF antennas , outboard limiter). b) New simplified WEST wall model, composed by axysimmetric surfaces and toroidally localized PFCs.

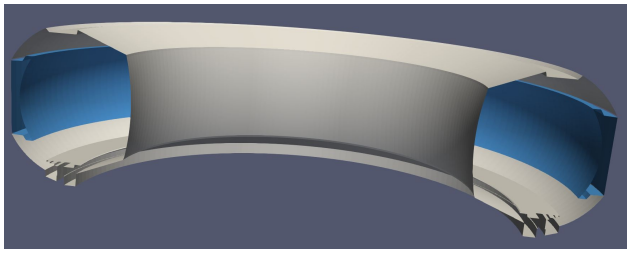

Figure 2: Previous WEST axisymmetric wall model, adopted in [5, 11]. The axisymmetric limiter/antenna can be seen (blue component in figure). To avoid overestimating recycling and erosion, due to the large surface of the limiter, this component was located at an arbitrary position far from the core.

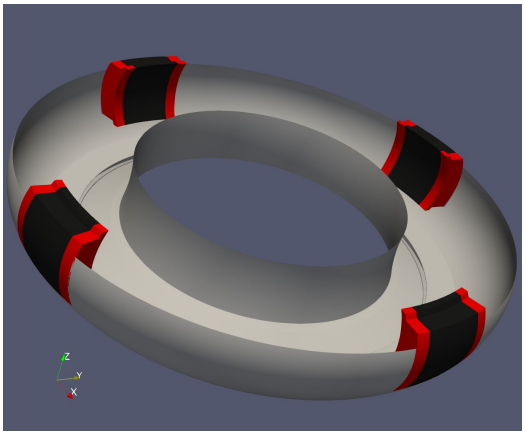

Figure 3: New WEST asymmetric wall model, including toroidally localized PFCs that can be seen as outboard limiters or antennas . The axysimmetric PFCs in figure (in grey) were always considered W sources, the black PFCs in figure were never considered W sources (modelling antennas components made by middle Z materials). Finally, the red PFCs W source was switched on and off to study its impact on W confined plasma contain, as they represented WEST W antennas protections.

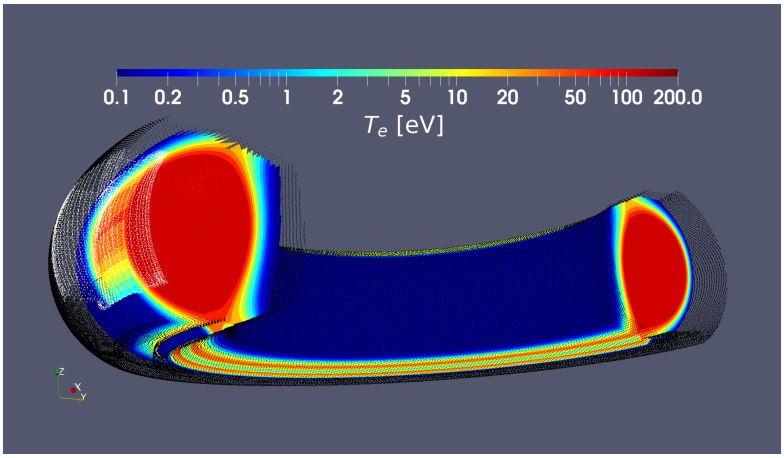


Figure 4: $T_e$ iso-surfaces on half of a torus, including only the surfaces with $T_e > 0.1$ [eV]. Black dots represent the axysimmetric part of the wall, white dots represent the toroidally localized objects. $T_e$ at antennas surface is similar to the one at the divertor plates (visible at the bottom of the torus).

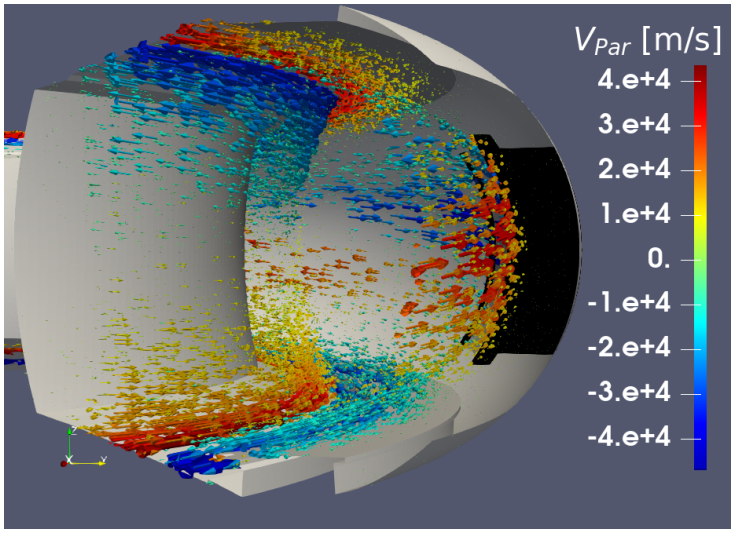


Figure 5: Plasma parallel velocity field seen from a torus poloidal cross section. The magnetic field enters in the figure plane, going in counterclockwise direction seeing the tokamak from the top. Red arrows go in the same direction of the magnetic field, blue arrows go in the counter direction.

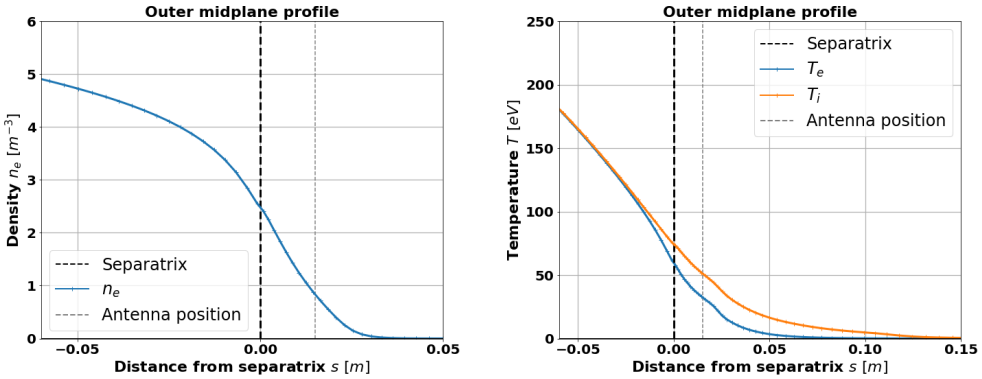


(a) (b)

Figure 6: SOLEDGE results midplane plots at a toroidal angle equidistant from two consecutive antennas for a) $n_{\mathrm{e}}$, and b) $T_{\mathrm{i}}$ and $T_{\mathrm{e}}$.

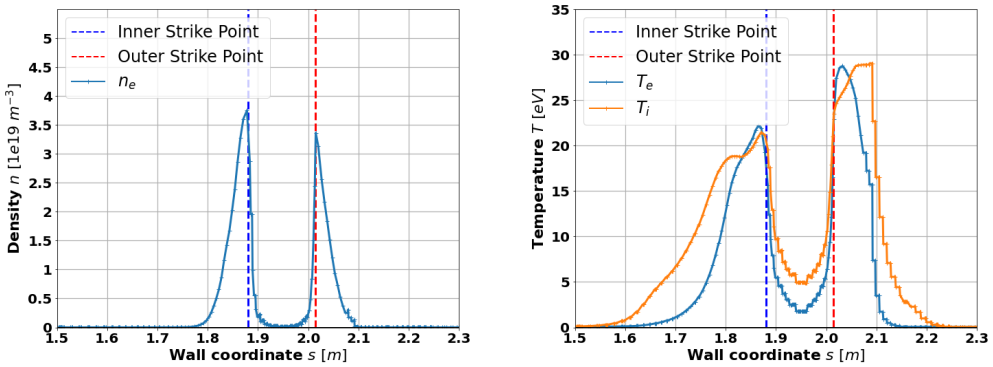


(a) (b)

Figure 7: SOLEDGE results divertor targets plots at a toroidal angle equidistant from two consecutive antennas for a) $n_{\mathrm{e}}$, and b) $T_{\mathrm{i}}$ and $T_{\mathrm{e}}$.

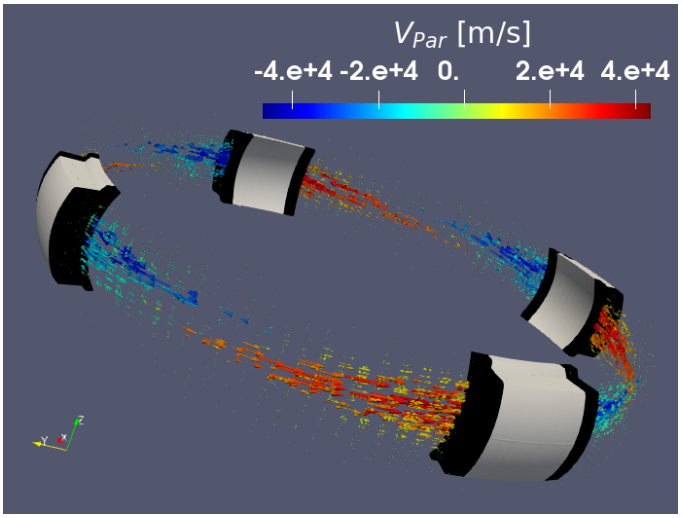


Figure 8: Plasma parallel velocity field at a major radius greater than the antennas one. Plasma parallel flow is slightly tilted in respect to the toroidal direction due to the poloidal component of the magnetic field.

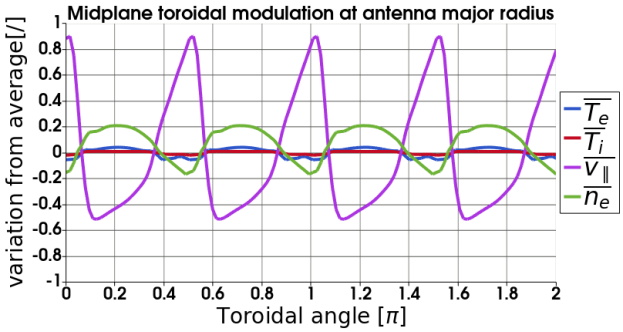


Figure 9: Relative midplane toroidal modulation of plasma physical quantities as defined in section 3. $T_\mathrm{i}$ and $T_\mathrm{e}$ vary from the average along the toroidal direction less than 0.05 times the maximum assumed value. The modulations are more important for $n_\mathrm{e}$ and $v_\parallel$.

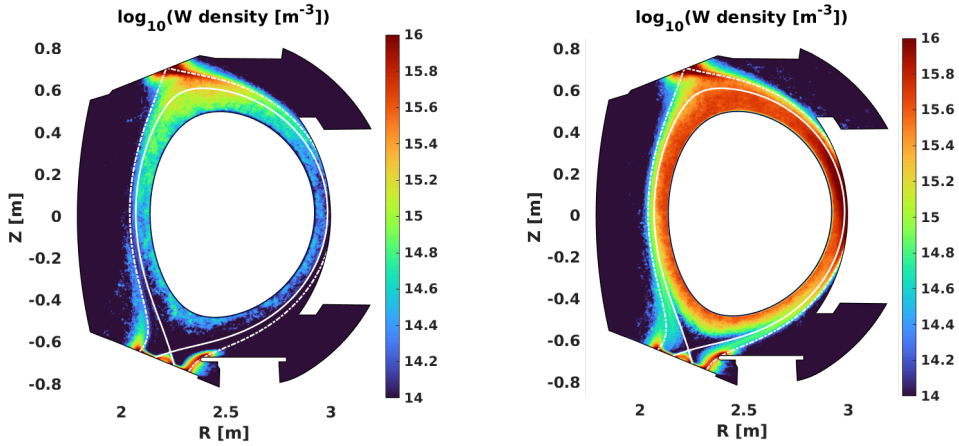


(a) (b)

Figure 10: W density maps: a) without considering antennas protections W erosion, and b) considering it.

# Tables

| | $<>_{2\pi}$ | $\mathrm{Max}()_{2\pi}$ |
|---|---|---|
| $T_\mathrm{e}$ [eV] | 31.4 | 31.8 |
| $T_\mathrm{i}$ [eV] | 55.2 | 55.8 |
| $n_\mathrm{e}$ [$10^{18}$ m$^{-3}$] | 6.0 | 7.0 |
| $v_\parallel$ [$10^4$ m s$^{-1}$] | 0.2 | 2.0 |

Table 1: Average and maximum values assumed by physical quantities along the toroidal angle $\varphi$ at the midplane at antenna major radius.

| | antennas protections | Rest of PFCs |
|---|---|---|
| Erosion rate [s$^{-1}$] | $3.27 \times 10^{19}$ | $2.54 \times 10^{20}$ |
| W ions inside separatrix [/] | $9.00 \times 10^{16}$ | $9.95 \times 10^{15}$ |

Table 2: Values comparison of ERO2.0 results. antennas protections contribute 90% of the overall W confined plasma content, but 85% of the erosion comes from the rest of the PFCs

# References


[1] A. Kallenbach et al. Non-boronized compared with boronized operation of ASDEX upgrade with full-tungsten plasma facing components. *Nuclear Fusion*, 49(4):045007, mar 2009.

[2] S. Brezinsek et al. Plasma-surface interaction in the Be/W/ environment: Conclusions drawn from the JET-ILW for ITER. *Journal of Nuclear Materials*, 463:11–21, 2015. PLASMA-SURFACE INTERACTIONS 21.

[3] J. Bucalossi et al. The WEST project: Testing ITER divertor high heat flux component technology in a steady state tokamak environment. *Fusion Engineering and Design*, 89(7):907–912, 2014. Proceedings of the 11th International Symposium on Fusion Nuclear Technology-11 (ISFNT-11) Barcelona, Spain, 15-20 September, 2013.

[4] G. Urbanczyk et al. RF wave coupling, plasma heating and characterization of induced plasma-material interactions in WEST L-mode discharges. *Nucl. Fusion*, 61, 2021.

[5] S. Di Genova et al. Modelling of tungsten contamination and screening in WEST plasma discharges. *Nuclear Fusion*, 61(10), 2021.

[6] A. Gallo et al. First efforts in numerical modeling of tungsten migration in WEST with SolEdge2D-EIRENE and ERO2.0. *Physica Scripta*, T171, jan 2020.

[7] Y. Marandet et al. Assessment of tungsten sources in the edge plasma of west. *Journal of Nuclear Materials*, 463:629–633, 2015. PLASMA-SURFACE INTERACTIONS 21.

[8] H. Bufferand et al. Numerical modelling for divertor design of the WEST device with a focus on plasma–wall interactions. *Nuclear Fusion*, 55(5):053025, apr 2015.

[9] J. Romazanov et al. Beryllium global erosion and deposition at JET-ILW simulated with ERO2.0. *Nuclear Materials and Energy*, 18:331–338, 2019.

[10] H. Bufferand et al. Three-dimensional modelling of edge multi-component plasma taking into account realistic wall geometry. *Nuclear Materials and Energy*, 18:82–86, 2019.

[11] A. Gallo et al. Interpretative transport modeling of the WEST boundary plasma: main plasma and light impurities. *Nuclear Fusion*, 60(12), nov 2020.

[12] G. Ciraolo et al. First modeling of strongly radiating west plasmas with soledge-eirene. *Nuclear Materials and Energy*, 20:100685, 2019.

[13] A. Huber et al. Understanding tungsten erosion during inter/intra-ELM periods in he-dominated JET-ILW plasmas. *Physica Scripta*, 96(12), 2021.

[14] G J van Rooij et al. Tungsten divertor sources in WEST related to impurity inventory and local plasma conditions. *Physica Scripta*, T171:014060, jan 2020.

[15] A. Eksaeva et al. ERO modelling of tungsten erosion in the linear plasma device PSI-2. *Nuclear Materials and Energy*, 12, 03 2017.

[16] I. Borodkina et al. Surface biasing influence on the physical sputtering in fusion devices. In *Journal of Physics: Conference Series*, volume 748, page 012002. IOP Publishing, 2016.

[17] R. Chodura. *Physics of Plasma-Wall Interactions in Controlled Fusion*. Springer New York, NY, 1986.

[18] P.C. Stangeby. *The Plasma Boundary of Magnetic Fusion Devices*. Series in Plasma Physics and Fluid Dynamics. Taylor & Francis, 2000.

[19] D. Reiser et al. Improved kinetic test particle model for impurity transport in tokamaks. *Nuclear fusion*, 38(2):165, 1998.

[20] Y. Homma et al. Numerical modeling of thermal force in a plasma for test-ion transport simulation based on monte carlo binary collision model. *Journal of Computational Physics*, 231(8):3211–3227, 2012.